THE JOURNAL OF PHYSICAL CHEMISTRY A

ARTICLE

pubs.acs.org/JPCA

Thermochemistry of Halomethanes CF_nBr_{4-n} ($n = 0-3$) Based on iPEPICO Experiments and Quantum Chemical Computations

Andras Bodi,[†] Ágúst Kvaran,[‡] and Bálint Sztáray[§,*]

[†]Paul Scherrer Institut, 5232 Villigen, Switzerland

[‡]Science Institute, University of Iceland, Dunhagi 3, 107 Reykjavík, Iceland

[§]University of the Pacific, Stockton, California 95211, United States

Supporting Information

ABSTRACT: Internal energy selected bromofluoromethane cations were prepared and their internal energy dependent fragmentation pathways were recorded by imaging photoelectron photoion coincidence spectroscopy (iPEPICO). The first dissociation reaction is bromine atom loss, which is followed by fluorine atom loss in CF_3Br and CF_2Br_2 at higher energies. Accurate 0 K appearance energies have been obtained for these processes, which are complemented by ab initio isodesmic reaction energy calculations. A thermochemical network is set up to obtain updated heats of formation of the samples and their dissociative photoionization products. Several computational methods have been benchmarked against the well-known interhalogen heats of formation. As a corollary, we stumbled upon an assignment issue for the ClF heat of formation leading to a 5.7 kJ mol^{-1} error, resolved some time ago, but still lacking closure because of outdated compilations. Our CF_3^+ appearance energy from CF_3Br confirms the measurements of Asher and Ruscic (J. Chem. Phys. 1997, 106, 210) and Garcia et al. (J. Phys. Chem. A 2001, 105, 8296) as opposed to the most recent result of Clay et al. (J. Phys. Chem. A 2005, 109, 1541). The ionization energy of CF_3 is determined to be 9.02−9.08 eV on the basis of a previous CF_3-Br neutral bond energy and the CF_3 heat of formation, respectively. We also show that the breakdown diagram of $CFBr_3^+$, a weakly bound parent ion, can be used to obtain the accurate adiabatic ionization energy of the neutral of 10.625 ± 0.010 eV. The updated 298 K enthalpies of formation Δ_fH°(g) for CF_3Br, CF_2Br_2, $CFBr_3$, and CBr_4 are reported to be −647.0 ± 3.5, −361.0 ± 7.4, −111.6 ± 7.7, and 113.7 ± 4 kJ mol^{-1}, respectively.

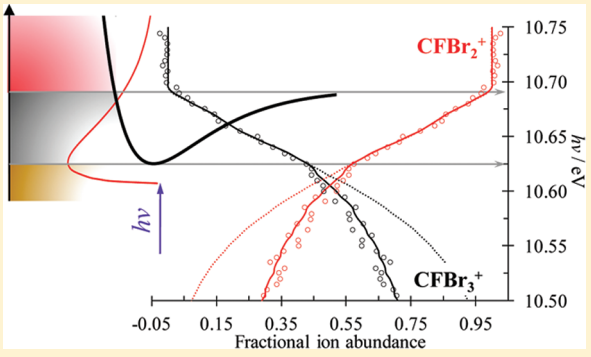

INTRODUCTION

The industrial use of brominated halomethanes has been significantly reduced, due to their ozone depleting and global warming potential (ODP and GWP dimensionless quantities with CFC-11 and CO_2, respectively, defined as 1). Large atmospheric lifetimes and weak C−Br bonds mean bromomethanes have ODP values around 0.4−16 well above the 0.2 limit in the Clean Air Act for phasing out a compound. The GWP of CF_3Br is in the 2800−8500 range.[1] Still, CF_3Br and CF_2Br_2 are among the most efficient fire suppressants by catalytically quenching radical chain reactions, mostly by H-radical scavenging.[2] For most uses, pentafluoroethane and heptafluoropropane are viable alternatives without ozone depletion effects but still with a GWP of 1100−6300. In contrast with halomethanes, these nearly perfluorinated alkanes act as somewhat less efficient noncatalytic inhibitors.[3,4] The energetics and accurate thermochemistry of brominated halomethanes help understand their radical quenching properties.

The CF_4 heat of formation is best known and will be used as an anchor in this study. Its value was reported to be $\Delta_fH^\circ_{0K} = -927.2 \pm 0.5$ kJ mol^{-1} and $\Delta_fH^\circ_{298K} = -933.4 \pm 0.5$ kJ mol^{-1} in the Third Millennium Ideal Gas and Condensed phase Thermochemical Database by Burcat and Ruscic.[5] Csontos et al. arrived at $\Delta_fH^\circ_{0K} = -927.8 \pm 2.0$ kJ mol^{-1} and $\Delta_fH^\circ_{298K} = -933.8 \pm 2.0$ kJ mol^{-1} on the basis of high level ab initio calculations.[6] We use the experimental 298 K value with the latest ab initio thermal enthalpy to arrive at $\Delta_fH^\circ_{0K} = -927.5 \pm 1$ kJ mol^{-1} in this study. The error bar of this value is somewhat arbitrary, because the two published thermal enthalpies, both proposed to be exact, differ by 0.2 kJ mol^{-1}. The remaining CF_nBr_{4-n} ($n = 0-3$) literature heats of formation are not used as anchors and can be summarized as follows. The heat of formation of CF_3Br was given as $\Delta_fH^\circ_{0K} = -636.9 \pm 2.9$ kJ mol^{-1} and $\Delta_fH^\circ_{298K} = -648.9 \pm 2.9$ kJ mol^{-1},[7] which was later revised to $\Delta_fH^\circ_{298K} = -649.77 \pm 2.1$ kJ mol^{-1} by Ruscic et al.[8] Burcat and Ruscic, however, list this value as $\Delta_fH^\circ_{298K} = -650.59 \pm 1.97$ kJ mol^{-1},

Received: August 20, 2011
Revised: October 9, 2011
Published: October 10, 2011

Table 1. Derived and Literature Heats of Formation and Calculated Thermal Enthalpies

	$\Delta_f H^\circ_{0K}$[a] / (kJ mol^{-1})	$\Delta_f H^\circ_{298K}$[a] / (kJ mol^{-1})		lit. $\Delta_f H^\circ_{298K}$	$H_{298K} - H_{0K}$ / (kJ mol^{-1})
CF_4				-927.5 ± 1[b]	12.8
CF_3Br	−635.0	−647.0	±3.5	-650.59 ± 1.97,[c] -636.9 ± 2.9,[d] -649.77 ± 2.1[e]	14.6
CF_2Br_2	−343.1	−361.0	±7.4	-379 ± 8[f]	16.4
$CFBr_3$	−87.7	−111.6	±7.7		18.4
CBr_4	143.3	113.7	±4	50.21−125.4[g]	20.6
CF_3^+	413.4[h]	410.2	±2	411.6 ± 1.96[c]	11.1
CF_2Br^+	619.0	596.9	±7.5		12.3
$CFBr_2^+$	826.1	821.9	±7.7		13.6
CBr_3^+	1031.8	1009.1	±4		15.1
$CHBr_3$				55.1 ± 2[i]	16.1
CH_3Br				-36.36 ± 0.42[j]	10.6
CH_4				-74.5 ± 0.06[k]	10.0
Br				111.9 ± 0.06[k]	6.2
F				79.37 ± 0.06[k]	6.5

[a] This work, 298 K values for the ions are obtained using the ion convention, i.e., $H_{298K} - H_{0K} = 0$ for the e^-. [b] Based on the Burcat[5] and Csontos[6] values (see text). [c] Burcat[5] value using the thermal electron convention, the ion convention value being 405.4 kJ mol^{-1}. [d] NIST-JANAF compendium.[7] [e] Ruscic et al.[8] [f] Lias et al.[9] [g] See refs 10−16 and the text for discussion. [h] Updated anchor in the thermochemical network. See text for discussion. [i] Shuman et al.[22] [j] Song et al.[69] [k] Active Thermochemical Tables.[70]

which corresponds to $\Delta_f H^\circ_{0K} = -638.48$ kJ mol^{-1}.[5] The error bar on the CF_2Br_2 heat of formation, $\Delta_f H^\circ_{298K} = -379 \pm 8$ kJ mol^{-1},[9] is the largest in this series, whereas the $CFBr_3$ heat of formation could not be found in the literature. Carbon tetrabromide, CBr_4, is quite extraordinary, because its published gas phase heats of formation span a large range. The NIST-JANAF compilation lists a calculated value from 1952 of $\Delta_f H^\circ_{298K} = 50.21$ kJ mol^{-1}.[7] The NBS thermochemical tables from 1968 give 79 kJ mol^{-1},[10] a Russian compilation from 1979 proposes 120 kJ mol^{-1}.[11] Papina et al. gave 115.8 ± 3.9 kJ mol^{-1},[12] a value disputed by Bickerton et al.,[13] who recommended 83.9 ± 3.9 kJ mol^{-1}. Several computational studies have attempted to tackle this issue: Oren et al. arrived at 119.2 kJ mol^{-1} in a relativistic ab initio study in 2004,[14] Marshall et al. used the QCISD(T) method with isodesmic reactions to obtain 110.6 kJ mol^{-1},[15] and most recently, Wang obtained 125.4 kJ mol^{-1} on the basis of the G3X atomization energy[16] (all values at 298 K). The literature values are also summarized in Table 1.

To improve and complement these thermochemical data, we set out to investigate the dissociative photoionization of these halomethanes in the vacuum ultraviolet (VUV) photon energy range. Internal energy selected $CF_nBr_{4-n}^+$ parent ions were prepared by threshold photoionization, and the unimolecular fragmentation pathways were recorded as a function of the ion internal energy. The lowest energy dissociation pathway in the halomethanes is the loss of a Br atom, $CF_nBr_{4-n} + h\nu \rightarrow CF_nBr_{3-n}^+ + Br + e^-$ ($n = 0-3$). The next, parallel dissociation reaction is a loss of a fluorine atom, $CF_nBr_{4-n} + h\nu \rightarrow CF_{n-1}Br_{4-n}^+ + F + e^-$ ($n = 2, 3$). The latter is in competition with the Br-loss process; i.e., the relative product abundances are determined by the ratio of the unimolecular dissociation rate constants. In $CFBr_3^+$, the F-loss process never competes with the Br loss efficiently, and only Br loss was observed for this species. Furthermore, the dissociative photoionization energy; i.e., the 0 K appearance energy for $CF_4 \rightarrow CF_3^+ + F + e^-$ cannot be measured with PEPICO, because the ground CF_4^+ ion state is repulsive in the Franck−Condon allowed energy region, and the CF_4^+ ion signal is only observed by dissociative photoionization of the dimer $(CF_4)_2$.[17−19] We measure the Br-loss process to be fast on the time scale of the experiment ($k > 10^7$ s^{-1}) meaning that all parent ions with more internal energy than the threshold will dissociate; i.e., there is no kinetic shift. The disappearance energy of the parent yields the dissociative photoionization energy in this case and can be determined with an accuracy of 0.3 kJ mol^{-1}.[20,21]

The experimental data for the second, parallel F-loss process yield the relative dissociation rates, which have to be modeled to obtain the corresponding 0 K appearance energies (E_0). As the photon energy approaches the F loss E_0 from above, the F-loss rate constant decreases to the limit dictated by the ion's density of states at E_0 internal energy and the appearance energy is obtained by extrapolation. First, an ab initio model rate curve is calculated for the first Br-loss step. The breakdown curves indicate the ratio of the dissociation rates in the energy region in which the two dissociation reactions compete; i.e., a derived model rate curve for the second dissociative photoionization process, $k_2(E)$, is thus obtained. The E_0 for the F loss is then found by extrapolating this $k_2(E)$ function, to where the dissociation rate vanishes. In a similar study on trihalides of methane, it has recently been found that modeling such processes in the rigid activated complex (RAC)-RRKM framework is a two-parameter problem with the E_0 difference determining the offset of the second process in the breakdown diagram and the activation entropy difference determining the shape (most importantly, the slope) of the corresponding breakdown curves.[22] The uncertainty of the second E_0 can be considerably larger than of the first step.

Whether merely configurational isomers[23] or stochiometrically different molecules,[22,25] halogenated hydrocarbons often lead to the same dissociative photoionization daughter ion. This is advantageous if the thermochemistry of the leaving neutral halogen atom is well-known, as it opens up the possibility of relating the heats of formation of the neutrals with the help of the appearance energies of the shared fragment ions via thermochemical cycles.

In the past, the dissociative photoionization of CF_3Br attracted the most interest for two reasons. First, because of its widespread application as fire suppressant, and second, there has been some

controversy over the ionization energy (IE) of the CF_3 radical. As the heat of formation CF_3Br is known, measuring the appearance energy of CF_3^+ yields the heat of formation of CF_3^+, which can be used in concert with the CF_3 heat of formation to determine the IE. Clay et al. first arrived at an appearance energy of 11.56 ± 0.02 eV,[26] which they revised in the latest experimental work on this quantity to 11.64 ± 0.04 eV.[24] In the meantime, Asher and Ruscic measured the E_0 to be 12.095 ± 0.005 eV,[27] and Garcia et al. published a value of 12.07 ± 0.02 eV.[28] In addition to computational evidence, namely the G3X-calculated E_0 = 12.15 eV by He and Wang,[29] we also wanted to obtain further experimental data to confirm or refute the most recent Clay at al. result. The dissociative photoionization of dibromodifluoromethane in the 8−22 eV photon energy range was studied by Seccombe et al.,[30] who reported room temperature appearance energies for Br loss (11.00 ± 0.05 eV) as well as for F loss (14.9 ± 0.2 eV). By adding the average thermal energy of 0.14 eV to these values, we derive E_0 values of 11.14 ± 0.05 and 15.04 ± 0.2 eV for Br and F loss, respectively. These values can be compared with the G3X-calculated ones of 11.22 and 12.91 eV, respectively.[29] To the best of our knowledge, the dissociative photoionization of $CFBr_3$ has not yet been studied experimentally, and the Br-loss appearance energy from CBr_4 has not been remeasured since 1974[31] either, in which study Werner et al. reported an E_0 of 10.47 ± 0.02 eV.

We would have preferred a purely experimental approach, in which the E_0 values leading to CF_3^+, CF_2Br^+, $CFBr_2^+$, and CBr_3^+ both by F and by Br loss are determined accurately and used to determine the relative heats of formation of the CF_nBr_{4-n} series. However, the two previously mentioned missing links, namely F losses from CF_4^+ and from $CFBr_3^+$, required us to turn to a combined experimental/theoretical approach.[32,33] This raises the question of a cost-effective and yet accurate computational method that can be used to calculate reliable isodesmic reaction energies. Because very few halogenated hydrocarbons have well-defined heats of formation, we turned to another compound family, interhalogens, of which the energetics are exceptionally well-known. A number of computational methods were benchmarked against the literature heats of formation of binary interhalogens. The ab initio isodesmic reaction networks were then evaluated at the most accurate level found, fc-CCSD/(SDB-)aug-cc-pVTZ//B3LYP/6-311+G(d), i.e., frozen core CCSD energies with the aug-cc-pVTZ basis set and the SDB large-core pseudopotential on Br at the B3LYP optimized geometries and zero-point energy correction with the 6-311+G(d) basis set.

EXPERIMENTAL SECTION

The X04DB beamline of the Swiss Light Source was used as the VUV source.[34] Higher order radiation was suppressed using a compact gas filter operated at 10 mbar with Ne or, at lower energies, with a Ne/Ar/Kr mixture, with an absorption path length of 10 cm. The sample was introduced into the imaging photoelectron photoion coincidence apparatus[35] (iPEPICO) through an effusive source at room temperature. The photon energy, with a resolution of about 2 meV, was calibrated against the well-known Ar and Ne autoionization lines in the same endstation. A constant 120 V cm^{-1} electric field was used to extract electrons and ions from the ionization region in opposite directions. The electrons are velocity map imaged[36,37] onto a DLD40 Roentdek detector with a better than 1 meV kinetic energy resolution at threshold. The mass analysis of the ions takes place in a two stage Wiley−McLaren[38] time-of-flight

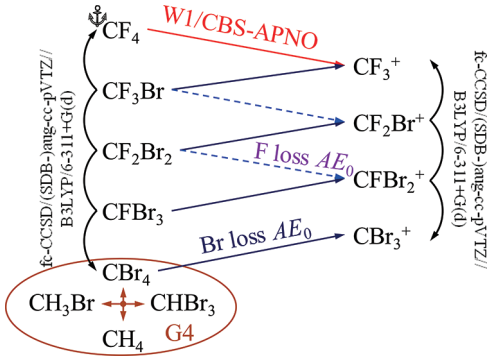

Figure 1. Combined experimental (AE_0) and computational (methods as indicated: W1, CCSD, CBS-APNO, G4) thermochemical network. The appearance energies interconnect the neutrals with the ions, ab initio isodesmic and Br_2/F_2 exchange reaction energies provide the neutral/neutral as well as ion/ion connections in the graph. CBr_4 is further connected to the $CH_3Br/CHBr_3/CH_4$ set by G4 isodesmic reaction energies.

(TOF) mass spectrometer for which the electron hits provide the start and the ion detector the stop signal. All electron and ion events were recorded and correlated on the fly to handle high count rates and maximize the signal-to-noise ratio.[39] The hot electron contamination of the center, threshold electron signal was determined by the energetic electron background in a small ring around the threshold region of the electron image and subtracted from the threshold signal.[40]

The threshold ionization TOF distributions are thus obtained as a function of photon energy. Thanks to the large ion residence time in the first acceleration region, unimolecular dissociation reactions with rate constants in the $10^3\ s^{-1} < k < 10^7\ s^{-1}$ range lead to asymmetric fragment ion peaks that unambiguously indicate if a kinetic shift has to be modeled.[41] We have not observed slow reactions in this study. The parent and fragment ion peaks can be integrated and the fractional ion abundances plotted in the breakdown diagram as a function of photon energy. In a first fast dissociation step, the ion internal energy distribution determines the breakdown diagram. All of the ions with more internal energy than the threshold will fragment. The threshold ionization cross sections are almost always constant over the thermal energy distribution of the neutral,[41] meaning that the internal energy distribution of the sample plus the photon energy less the adiabatic ionization energy yields the parent ion internal energy distribution. Consequently, the disappearance energy of the parent ion, i.e., when the zero internal energy neutrals also gain enough energy to dissociate, is equal to the E_0. Yet the whole breakdown diagram is modeled to obtain more reliable thresholds. If, as is the case for CBr_4^+ and $CFBr_3^+$ (see below), the potential energy well of the ion is so shallow that the room temperature internal energy distribution of the neutral does not fit in it, the whole neutral internal energy distribution cannot be transposed to the bound ground state ion manifold. This has the added benefit that the breakdown curve can be used to determine the adiabatic ionization energy of the sample. CF_3Br was obtained from Pfaltz and Bauer, CBr_4 and CF_2Br_2 from Sigma−Aldrich, and $CFBr_3$ from Alfa Aesar, and they were used without further purification.

COMPUTATIONAL APPROACH

The calculations were carried out using Gaussian 09.[42] Because the appearance energy of F loss from CF_4^+ and from

CF_3Br^+ could not be measured, the experimental thermochemical network is disconnected. This can be remedied by invoking accurate quantum chemical calculations. Isodesmic reaction energies can be calculated much more accurate than ab initio appearance energies.[43] Hence, two networks were set up, one for the sample compounds and one for the fragment ions as illustrated in Figure 1. In addition to the three independent isodesmic reaction energies connecting CF_nBr_{4-n} ($n = 0-4$), and the two reaction energies connecting $CF_nBr_{3-n}^+$ ($n = 0-3$),

$$CF_nBr_{4-n} + CF_{n-2}Br_{6-n} \rightarrow 2CF_{n-1}Br_{5-n} \quad (n = 2-4) \quad (1)$$

$$CF_nBr_{3-n}^+ + CF_{n-2}Br_{5-n}^+ \rightarrow 2CF_{n-1}Br_{4-n}^+ \quad (n = 2, 3) \quad (2)$$

the Br_2/F_2 exchange reaction energies

$$CF_nBr_{4-n} + 1/2Br_2 \rightarrow CF_{n-1}Br_{5-n} + 1/2F_2 \quad (n = 1-4) \quad (3)$$

were also considered. The heat of formation of CBr_4 was further anchored to CH_3Br and $CHBr_3$ by G4[44] isodesmic reaction energies.

Our goal was not to use a rigorous and very expensive computational approach like, e.g., HEAT,[45] but rather to find a reasonably exhaustive method delivering as accurate relative energies as possible. In contrast with halogenated hydrocarbons, most interhalogens have long had very well-defined heats of formation, based on equilibrium and spectroscopic measurements with uncertainties sometimes below 0.1 kJ mol^{-1}.[7] The 0 K formation energies of the interhalogens ClF, ClI, BrF, BrCl, and BrI from the gas phase halogens F_2, Cl_2, Br_2, and I_2 were calculated with several methods, such as density function theory (DFT) with the B3LYP[46] and M06[47] functionals and the 6-311+G(d) basis set, frozen core fc-CCSD, fc-CCSD(T) with the (SDB-)aug-cc-pVTZ and (SDB-)aug-cc-pVQZ[48,49] as well as the aug-cc-pV5Z-PP[50] basis sets with an effective core potential (ECP) on Br and I, as well as without the ECP. Core-correlation was taken into account at the MP2 and CCSD levels. The W1,[51] CBS-QB3,[52] and G4[44] composite methods were also used where applicable. Detailed results are available as electronic Supporting Information.

The computed reaction energies were first compared to the literature based values, and the best performing three methods are listed here. The smallest sum of differences squared for the five interhalogens, $\varepsilon^2 = \Sigma(\Delta_rH^{ref} - \Delta_rH^{calc})^2/(\text{kJ mol}^{-1})^2$, was obtained for B3LYP/6-311+G(d) results, $\varepsilon^2 = 138$, the next higher being fc-CCSD/(SDB-)aug-cc-PVTZ//B3LYP/6-311+G(d), $\varepsilon^2 = 159$, followed by fc-CCSD(T)/aug-cc-pV5Z//B3LYP/6-311+G(d), $\varepsilon^2 = 195$. In the next step, the interhalogen heats of formation were optimized to minimize the total error function, $\Sigma\varepsilon^2$; i.e., each method was then compared to the average computed reaction energies. The difference between the average computed and the literature 0 K heats of formation was determined to be −5.4, 0.9, −1.1, −1.2, and +1.0 kJ mol^{-1} for ClF, ClI, BrF, BrCl, and BrI, respectively. On the one hand, this serves to illustrate the expected accuracy of these methods, whereas on the other, we believe that the difference in the ClF $\Delta_fH^\circ_{0K}$ actually reflects a −5.7 kJ mol^{-1} error in the ClF heat of formation. fc-CCSD/(SDB-)aug-cc-PVTZ//B3LYP/6-311+G(d) results agree best with the average computed value with $\varepsilon^2 = 2.9$. fc-CCSD/(SDB-)aug-cc-PVQZ//B3LYP/6-311+G(d) results yield $\varepsilon^2 = 20.5$ and B3LYP/6-311+G(d) has $\varepsilon^2 = 61.5$. Although intended to be a simple benchmarking exercise to find the most suitable method for the $CF_nBr_{4-n}/CF_nBr_{3-n}^+$ systems, the particularly large difference we found between the computed and published $\Delta_fH^\circ_{0K}(ClF)$ prompted us to look into this matter, as well.

The NIST-JANAF Thermochemical Tables list $\Delta_fH^\circ_{298K}(ClF) = -50.29 \pm 0.42$ kJ mol^{-1} and $\Delta_fH^\circ_{0K}(ClF) = -50.20 \pm 0.42$ kJ mol^{-1}. The ClF heat of formation is based on spectroscopic measurements by Wahrhaftig[53] and by Schmitz and Schumacher,[54] indicating a band convergence limit of 21 514 ± 10 cm^{-1}, which was assigned to the products $Cl(^2P_{1/2}) + F(^2P_{3/2})$, corroborated by a dissociative ionization threshold reported by Dibeler et al.,[55] and disputed by Nordine,[56] who argued for an $Cl(^2P_{3/2}) + F(^2P_{1/2})$ assignment. Even though the NIST-JANAF compilation makes no mention of this conundrum, the question still seemed unsettled to Coxon.[57] On the basis of the predissociation behavior of ClF, McDermid arrived at the conclusion that the $Cl(^2P_{3/2}) + F(^2P_{1/2})$ assignment was correct.[58] The difference between the two asymptotes being 478 cm^{-1}, this means that the heat of formation of ClF should be 5.72 kJ mol^{-1} lower than that reported by Chase.[7] Furthermore, using the updated fluorine and chlorine bond energies of $D_0^\circ(Cl_2) = 242.604$ kJ mol^{-1} and $D_0^\circ(F_2) = 154.78$ kJ mol^{-1},[5] and McDermid's assignment yields $\Delta_fH^\circ_{298K}(ClF) = -55.97 \pm 0.42$ kJ mol^{-1} as well as $\Delta_fH^\circ_{0K}(ClF) = -55.88 \pm 0.42$ kJ mol^{-1}. This agrees with the value reported by Burcat.[5]

When compared with the NIST-JANAF values and the updated ClF heat of formation, the error function is $\varepsilon^2 = 21.1$ for fc-CCSD/(SDB-)aug-cc-PVTZ//B3LYP/6-311+G(d), $\varepsilon^2 = 39.5$ for fc-CCSD/(SDB-)aug-cc-PVQZ//B3LYP/6-311+G(d) and $\varepsilon^2 = 71.1$ for the all-electron ae-CCSD/aug-cc-pV5Z(-PP)//B3LYP/6-311+G(d) calculation. Thus, fc-CCSD/(SDB-)aug-cc-PVTZ//B3LYP/6-311+G(d) reaction energies were used in the computational part of the thermochemical network.

The appearance energy for $CF_4 \rightarrow CF_3^+ + F + e^-$ was also determined in silico, i.e., using quantum chemical calculations. The W1 and CBS-APNO[59] reaction energies for $CF_4 \rightarrow CF_3^+ + 1/2\ F_2 + e^-$ indicate an E_0 of 14.716 and 14.694 eV, respectively. Recently, Forysinski et al. have obtained the 0 K appearance energy of H loss from the ion of CH_2F_2 as 13.065 ± 0.003 eV.[60] The W1 and CBS-APNO calculated values are 13.077 and 13.062 eV, respectively. By weighting the W1 and CBS-APNO values to reproduce the experimental E_0 for H loss from CH_2F_2, we arrive at $E_0 = 14.699$ eV for F-loss from CF_4. On the basis of the standard deviation of the W1, CBS-APNO and CCSD results (1.3 kJ mol^{-1}), we suggest this value is more accurate than ±2 kJ mol^{-1}. Using $\Delta_fH^\circ_{0K}(CF_4) = -927.5 \pm 1$ kJ mol^{-1}, this leads to $\Delta_fH^\circ_{0K}(CF_3^+) = 413.4 \pm 2$ kJ mol^{-1}.

RESULTS AND DISCUSSION

Modeling the Fast First Dissociation Step. The breakdown diagrams for Br loss from CF_3Br, CF_2Br_2, $CFBr_3$, and CBr_4 are shown in Figure 2. These processes are fast; thus, in the first approximation, the breakdown curves correspond to the cumulative distribution function (CDF) of the neutral molecule's internal energy distribution with the daughter ion abundance reaching unity at E_0.[41] However, this assumption is only reasonable if the potential energy well is deep enough that the whole of the energy distribution can be transposed to the ionic manifold

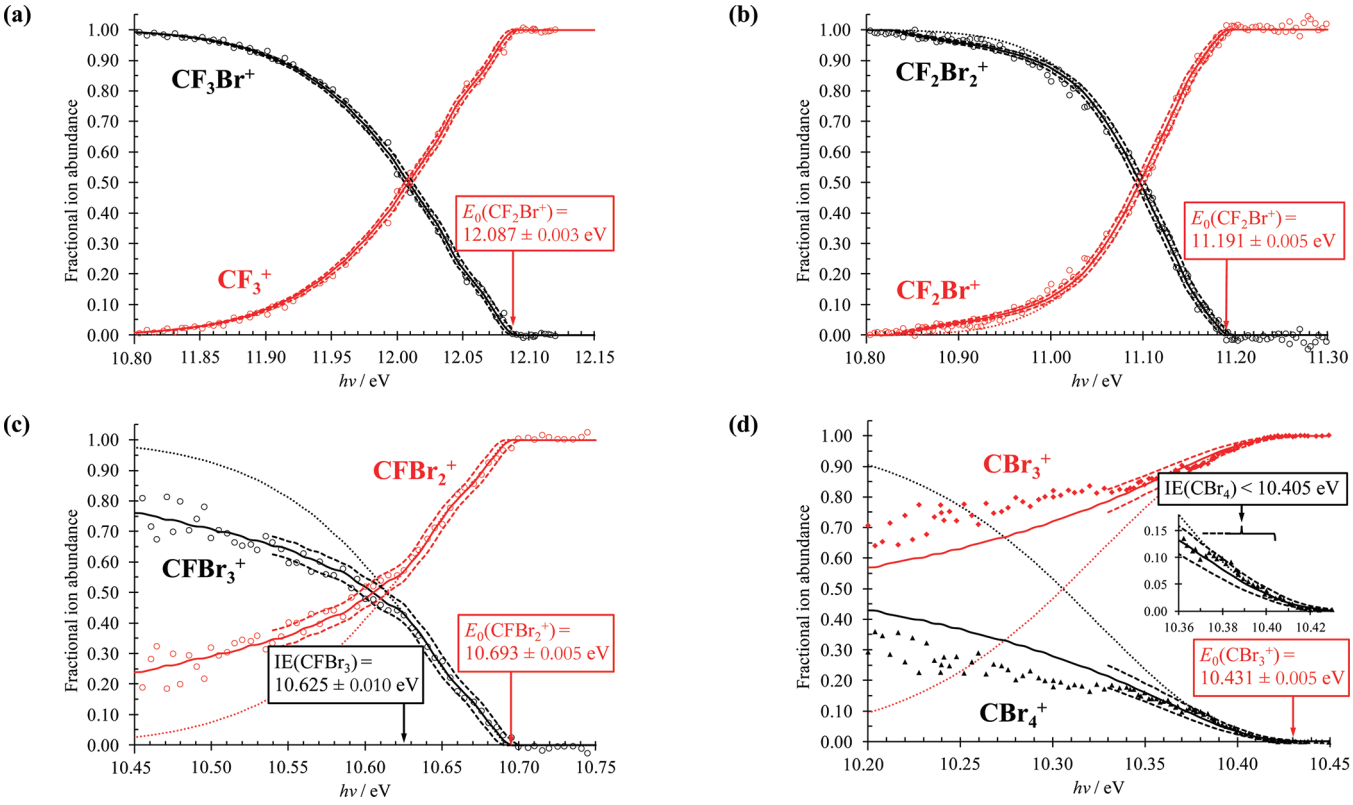

Figure 2. Breakdown diagrams corresponding to Br loss in (a) CF_3Br, (b) CF_2Br_2, (c) $CFBr_3$, and (d) CBr_4. The circles correspond to measured fractional ion abundances; the continuous lines to the modeled curves used to obtain the 0 K appearance energies. Additionally, the dotted curves in (c) and (d) are simulated results with large Br-loss barriers so that the room temperature thermal energy distribution of the neutral fits in the potential energy well. The dashed curves show the uncertainty limits. The 0 K appearance energies as well as the adiabatic ionization energies for $CFBr_3$ and CBr_4 are marked.

before dissociation occurs. If, however, the width of the thermal energy distribution is larger than the depth of the potential energy well, the parent ion fractional abundance can never reach 100%. Among the four molecules studied here, this is quite evident from the experimental breakdown curves of CBr_4^+ and $CFBr_3^+$. For these molecules, the potential energy well is much shallower than the width of the neutral internal energy distribution and the lowest energy neutrals will not contribute to the ion signal (Figure 3). If the Franck−Condon factors are still approximately uniform across the energy distribution (where ionization is possible), the breakdown curve can be modeled as the ratio of the internal energy distribution in the potential energy well vs above it, cutting off the part of the energy distribution that falls below the adiabatic ionization energy. Therefore, the breakdown curve depends on the adiabatic ionization energy, which can thus be obtained, presumably more reliably than from the threshold photoelectron spectrum. A simpler way is to model the breakdown curve by assuming a deep enough potential energy well, and the photon energy at which the calculated curve deviates from the experimental curve is taken as the adiabatic IE. In the case of $CFBr_3$, both methods yield the same IE, 10.625 ± 0.010 eV, which is an encouraging sign that using the breakdown diagram is a sound method for obtaining the adiabatic IE. Furthermore, the experimental breakdown curve shows some structure that is quite well reproduced by the modeled curves, calculated from the density of state function of the neutral molecule with a fine structure due to the

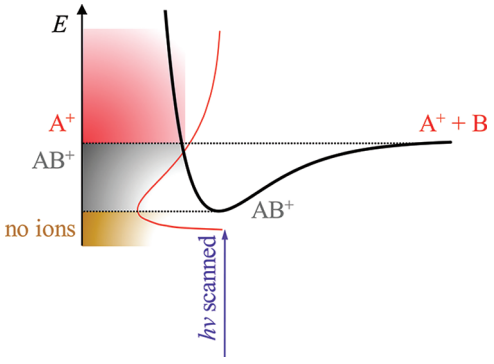

Figure 3. In loosely bound ionic systems the breakdown diagram can be used to determine the ionization energy. As the photon energy, $h\nu$, is scanned, the parent ion fractional abundance corresponds to the normalized parent ion internal energy distribution integral from zero to the barrier, whereas the daughter ion fractional abundance is given by the integral from the barrier to infinity. Thus, the breakdown diagram deviates from its presumed (deep-well) shape below the adiabatic ionization energy.

spacing of the vibrational levels. For CBr_4^+, the situation is slightly more difficult as the barrier to dissociation is so low that only a small fraction of the ion distribution leads to the CBr_4^+ parent ion. Considering the mediocre signal-to-noise ratio in the breakdown curve, the purely thermal modeled curve deviates

dx.doi.org/10.1021/jp208018r |J. Phys. Chem. A 2011, 115, 13443–13451

from the experimental data at around 10.375 eV while assuming this IE does not lead to a satisfactory modeled breakdown curve. Assuming an IE of 10.405 eV gives a fairly good modeled curve down to 10.33 eV, which then deviates significantly at photon energies far below the ionization energy. Apparently, in this case, the method of obtaining the ionization energy from the breakdown curve is likely to yield only a firm upper limit for the ionization energy of 10.405 eV, whereas a lower limit for this value is much less certain and is likely to be around where the thermally modeled curve deviates from the experimental data points, at 10.375 eV. However, unfavorable Franck−Condon factors to the ionic minimum can complicate the issue here. The breakdown curve based adiabatic ionization energies can be compared with the previous values of 10.67 ± 0.01[61] and 10.31 ± 0.02 eV[31] for $CFBr_3$ and CBr_4, respectively. In the case of CF_2Br_2, the modeled breakdown curve is much less sensitive to the assumed adiabatic IE, the deep-well limit only deviates from the experimental breakdown curve at low photon energies, between 11.0 and 11.05 eV. Assuming a room temperature energy distribution of the neutral precursor and fitting the adiabatic to a good agreement between the low-E part of the modeled and experimental breakdown curves gives an approximate IE of 11.035 ± 0.05 eV, which can be compared with 10.98 ± 0.02 eV as reported by Wang and Leroi.[62]

The 0 K appearance energies were obtained by the fitting procedure for fast dissociations as described elsewhere.[41] For CF_2Br_2, $CFBr_3$, and CBr_4, the effect of the low lying barrier and, thus, incomplete ionization of the neutral energy distribution were taken into account. The experimental 0 K appearance energies for Br loss from CF_3Br, CF_2Br_2, $CFBr_3$, and CBr_4 are 12.087 ± 0.003, 11.191 ± 0.005, 10.693 ± 0.005, and 10.431 ± 0.005 eV, respectively. Although the disappearance of the parent ion in the latter is much more gradual than for the first three, this latter error bar is equally good because of the very little noise on this set of experimental data. The CF_3Br result is between the Asher and Ruscic[27] and Garcia et al.[28] values, suggesting that both measurements were correct; only their mutually exclusive error bars were too optimistically set. This onset, together with the neutral C−Br bond energy in CF_3Br of 3.070 ± 0.013[63,64] (3.070 ± 0.030 eV[8]) yields a CF_3^+ ionization energy of 9.02 ± 0.03 eV. This can be compared with the 9.08 ± 0.03 eV value on the basis of the CF_3^+ (4.285 ± 0.020 eV) and CF_3 (−4.796 ± 0.021 eV)[8] heats of formation. The CF_2Br_2 result is just at the high limit of the Seccombe value,[30] although the conversion of 298 K appearance energies to 0 K is somewhat arbitrary, thus making the comparison unclear. The Br-loss appearance energy by Werner at al.[31] appears to be 0.03 eV too high.

Modeling the Second, Parallel Dissociation Step. A second dissociation pathway, the loss of a fluorine atom, was observed in CF_3Br^+ and $CF_2Br_2^+$. In $CFBr_3^+$, CCSD calculations predict a 0.03 eV smaller E_0 difference between the F- and Br-loss processes than in CF_2Br_2, so the absence of F loss in the former is in fact surprising. It is nevertheless corroborated by the relative intensities of the corresponding peaks in the electron ionization mass spectra.[65] A possible explanation could be that the small, 6 kJ mol^{-1}, barrier to Br loss and the consequently highly repulsive character of the ground state ion potential energy surface in $CFBr_3^+$ means that, at higher energies, the dissociation is impulsive and Br atoms are preferentially lost.

The branching ratios between Br loss and F loss are determined by the ratio of the rate constants in the energy range in which both channels are open. In the statistical framework,

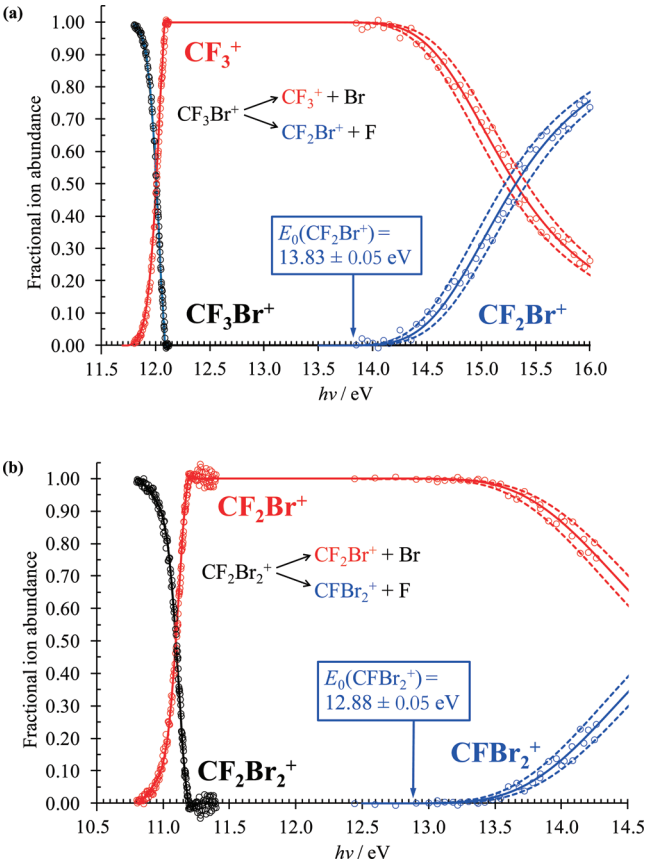

Figure 4. Experimental breakdown diagram corresponding to the second, F-loss process in (a) CF_3Br and in (b) CF_2Br_2 (circles) shown together with the RAC-RRKM model and its uncertainty limits (continuous lines).

$k_1(E)/k_2(E) = N_1^{\ddagger}(E - E_0(1))/N_2^{\ddagger}(E - E_0(2))$; i.e., the relative rates are a function of the transition state number of states. This means that whereas, due to the energy selection of the PEPICO setup, the first appearance energy can be determined to an accuracy that is limited mainly by the photon energy resolution, the appearance energy of the second, parallel dissociation is model dependent. In the modeling of these halon data, we used two rate theories to determine the second dissociative photoionization onset: the rigid activated complex (RAC-)RRKM, as well as the simplified statistical adiabatic channel model (SSACM), which can be practically formulated starting from phase space theory (PST). In the former, the transitional modes in the transition state are treated as harmonic oscillators, and the transition state is fixed, whereas in the SSACM, the number of states of the transitional modes are calculated as in PST and then scaled with an energy-dependent scaling factor, as described earlier.[41,66,67]

The RRKM modeling of the second dissociation was fairly straightforward along the lines of an earlier work on a set of haloforms.[22] Briefly, the slope of the second fragment ion's relative abundance curve depends on the difference of the two activation entropies and it is largely independent of their absolute values. In both cases, the steepness of the second breakdown curve indicates that the fluorine-atom-loss dissociation goes through a looser transition state than Br loss. Figure 4 shows the experimental breakdown curves in the entire photon energy region of interest, along with the results of the modeling.

The dashed lines, similarly to the modeling of the first dissociations, earlier, indicate the rather generous error bars on the determined second 0 K appearance energies. The derived E_0 values for F loss in CF_3Br and CF_2Br_2 are 13.83 ± 0.05 and 12.88 ± 0.05 eV, respectively.

The functional form of the SSACM rate constant is based on PST, but it adds an adjustable function that prevents the rate constant from rising too rapidly with increasing ion internal energy. This energy-dependent rigidity factor accounts for the anisotropy of the potential energy surface.[67] The functional form of this rigidity factor depends on the type of dissociation. For ionic fragmentations that are dominated by valence forces at short range and by comparatively weak ion-induced dipole forces at long range, a simple exponential decay-type rigidity factor can be used. However, as pointed out earlier,[68] this results in an unphysical behavior at higher internal energies, where the exponential scaling of the number of states of the transitional modes results in a $k(E)$ curve with negative slope. Therefore, the following function offers a better scaling factor by ensuring that it cannot be arbitrarily small that would result in an unphysical rate curve.

$$f_{\text{rigid}}(E) = (1 - f_\infty) \exp\left(-\frac{E - E_0}{c}\right) + f_\infty \quad (4)$$

where c is an adjustable parameter and the functional form of f_∞ is discussed below.

In the first approximation, the minimum value of the rigidity factor, f_∞, can be a constant value; however, as at high energies the transition state "moves in", RAC-RRKM-like behavior is expected. Therefore, the functional form of f_∞ has to reflect the ratio of the RAC-RRKM and the PST numbers of states. In the classical limit, this results in the following formula for a dissociation leading to a spherical top and an atom:

$$f_\infty(E) = \frac{B_\infty (E - E_0)}{2h\nu_1 h\nu_2} \quad (5)$$

where B_∞ is the geometrical mean of the rotational constants of the spherical top and $h\nu_i$ are the high-E limit of the transitional vibrational frequencies. For dissociations with a different number of transitional modes, similar formulas can be obtained, and f_∞ scales as the $(n/2)$th power of $E - E_0$, where n is the number of transitional modes.

If one assumes that, at high energies, RRKM provides a reliable rate constant, the predictions of the SSACM calculations, as formulated above, can be compared to the RRKM rates or numbers of state. These calculations suggest that using reasonable estimates for the two transitional vibrational frequencies results in too small numbers of states and the denominator of eq 5 has to be treated as a variable parameter and optimized at high energies so that the slope of the SSACM rate curve agrees with the RAC-RRKM curve. Because the optimal value for the denominator also depends on the c constant in eq 4, the SSACM model has three adjustable parameters, making the search for a global minimum more difficult, and during the fitting procedure, large changes either in the denominator of eq 5 or in the c parameter are counteracted by changes in the other. The RAC-RRKM model has two physical parameters, ΔE_0 and $\Delta\Delta S^{\ddagger}$, for two observables, i.e., the relative position and the slope of the breakdown curve of the second daughter. Introducing a third parameter with limited physical meaning in the SSACM model leads to a less well-defined model, which yields 0 K appearance energies for F loss of 13.84 ± 0.15 and 12.91 ± 0.15 eV, in CF_3Br and CF_2Br_2, respectively. Although the crucial, low-energy part of the rate curve is only extrapolated for the second parallel process, and there are no standard and proven methods to extract appearance energies for such dissociations, the fact that the extrapolation is over a relatively small energy range and the agreement between the SSACM and RAC-RRKM models are encouraging. Thus, we propose 13.84 ± 0.05 and 12.90 ± 0.1 eV as the F-loss E_0 values in CF_3Br and CF_2Br_2.

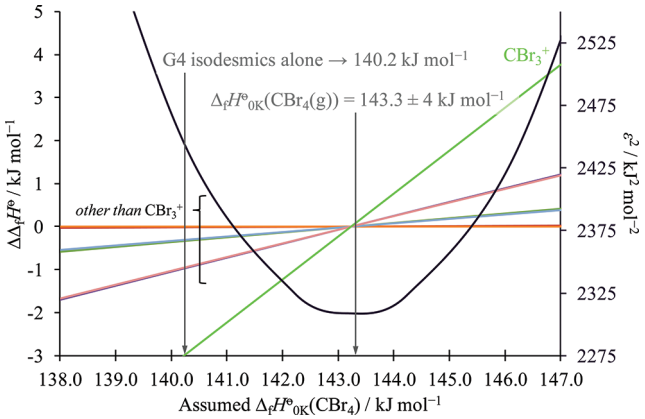

Figure 5. Effect of $\Delta_f H^\circ_{0K}(CBr_4)$ on the error function in the thermochemical network as well as on the other derived heats of formation. In addition to the well-defined minimum, only the CBr_3^+ heat of formation depends strongly on $\Delta_f H^\circ_{0K}(CBr_4)$, as the network dampens the propagation of its variation into the rest of the parameters. The unassigned colored lines show that changes in the CBr_4 heat of formation do not propagate into any of the other network components' $\Delta_f H$ results.

Sensitivity Analysis and Enthalpies of Formation. The thermochemical network in Figure 1 consists of the experimental 0 K appearance energies for the first and second dissociation channels together with the ab initio reaction energies. The CF_4 heat of formation is used as anchor, and the CF_3^+ heat of formation is also held constant in the analysis. The overall heat of formation range is spanned by $\Delta_f H^\circ(CBr_4)$, for which a number of different values have been proposed in the literature. Therefore, $\Delta_f H^\circ(CBr_4)$ is a fit parameter in the analysis. At the same time, the relative weights of experimental vs computed energies can also be varied. Within the experimental data set, the first and second appearance energies have different error bars. To take this into account, the error function for the appearance energies is multiplied by 10 meV/δ, where δ is the experimental error bar. The network is defined by the 0 K heats of formation of the constituent molecules and ions, and the error function (ε^2) is obtained as the weighted sum of the differences squared between the measured appearance energies/calculated reaction energies and the $\Delta_f H^\circ$-calculated energy differences within the network. Detailed results are available as Supporting Information.

The effect of the assumed $\Delta_f H^\circ(CBr_4)$ on the goodness of fit as well as on the other heats of formation is shown in Figure 5. First, the uncertainty in the CBr_4 heat of formation has little effect on the other heats of formation with the exception of CBr_3^+. Second, the error function shows a well-defined minimum at $\Delta_f H^\circ_{0K}(CBr_4)$ = 143.3 kJ mol^{-1}, corresponding to $\Delta_f H^\circ_{298K}(CBr_4)$ = 113.7 kJ mol^{-1}. Based on the good agreement with the purely G4 value, this value is most likely accurate to within 4 kJ mol^{-1}.

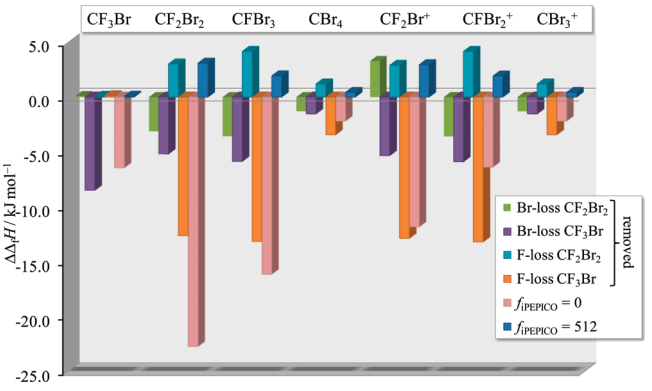

Figure 6. Sensitivity of the thermochemical network to the weight of the experimental data ($f_{iPEPICO}$) as well as removal of individual data points. The graph shows the change in the best fit heats of formation with respect to the balanced ($f_{iPEPICO}$ = 128) fit with all experimental data points.

The fit sensitivity to the experimental data points and the weight of the experimental results is shown in Figure 6. We consider the $f_{iPEPICO}$ parameter space, i.e., the weight of the experimental points in the error function, as well as removing individual data points from the fit. The balanced fit is taken as $f_{iPEPICO}$ = 128, in addition to $f_{iPEPICO}$ = 512 and $f_{iPEPICO}$ = 0. The effect of removing the experimental Br-loss appearance energy for CF_2Br_2 and CF_3Br as well as the each F-loss appearance energy are also shown in Figure 6. The other two Br-loss E_0 values do not have a significant effect on any of the heats of formation. The inclusion of the F-loss E_0 from CF_3Br has a significant effect on the heats of formation of CF_2Br_2, $CFBr_3$, CF_2Br^+, and $CFBr_2^+$. The calculations alone predict these species to be ca. 10−15 kJ mol^{-1} more stable. Consequently, the error bars for these species resulting from fit uncertainties are set to 7 kJ mol^{-1}, whereas we estimate a 3 kJ mol^{-1} contribution for the other species. Thus, the uncertainties in the thermochemical network come from (1) the 1 kJ mol^{-1} error bar on CF_4, (2) the 2 kJ mol^{-1} error bar on CF_3^+, (3) the 4 kJ mol^{-1} error bar on CBr_4, and (4) the uncertainty arising from the instability of the thermochemical network with respect to removing experimental nodes from it. These were taken into account in deriving the heats of formation as listed in Table 1.

CONCLUSIONS

The thermochemistry of the CF_nBr_{4-n} species was studied by imaging photoelectron photoion coincidence spectroscopy (iPEPICO) as well as ab initio isodesmic calculations. A thermochemical network was set up, in which the neutral and the ionic subnetworks are intraconnected by computed reaction energies and interconnected by experimental 0 K dissociative photoionization, i.e., appearance energies. An error function was defined, and the heats of formation are obtained by minimizing the error function. To estimate their uncertainties and to pinpoint the best approach, several computational methods were benchmarked against known interhalogen enthalpies of formation. In this process, the ClF heat of formation was found to be misreported by 5.7 kJ mol^{-1} (cf. the claimed error bar of 0.4 kJ mol^{-1}), a discrepancy resulting from the erroneous assignment of spectroscopic measurements, and pointed out before. In addition to the newly determined heat of formation of $CFBr_3$ and the dissociative photoionization products, the updated neutral heats of formation are also summarized in Table 1. Furthermore, the breakdown diagram of weakly bound parent ions, such as $CFBr_3^+$ and CBr_4^+, was shown to be useful in determining accurate adiabatic ionization energies.

ASSOCIATED CONTENT

Supporting Information. Detailed computed energies for the benchmarking of computational methods as well as the thermochemical network data can be downloaded. This information is available free of charge via the Internet at http://pubs.acs.org.

AUTHOR INFORMATION

Corresponding Author
*E-mail: bsztaray@pacific.edu.

ACKNOWLEDGMENT

We are grateful to Ingvar Arnason for his help with sample procurement. Huasheng Wang and Sampada N. Borkar have contributed to running the iPEPICO experiment; their support is greatly appreciated. This work was supported by the ACS Petroleum Research Fund. The financial support by the Swiss Department of Energy (BFE #100708) is also gratefully acknowledged. The experimental work was carried out at the VUV beamline of the Swiss Light Source of the Paul Scherrer Institut. The research leading to these results has received funding from the European Community's Seventh Framework Programme (FP7/2007-2013) under grant agreement n.°226716.

REFERENCES

(1) Daniel, J. S.; Velders, G. J. M. Halocarbon scenarios, ozone depletion potentials, and global warming potentials, Chapter 8. In *Scientific Assessment of Ozone Depletion: 2006*; Global Ozone Research and Monitoring Project, Report No. 50; World Meteorological Organization: Geneva, Switzerland, 2007.

(2) Westbrook, C. K. *Combust. Sci. Technol.* **1983**, *34*, 201–225.

(3) Williams, B. A.; L'Espérence, D. M.; Fleming, J. W. *Combust. Flame* **2000**, *120* (1−2), 160–172.

(4) Shebeko, Y. N.; Azatyan, V. V.; Bolodian, I. A.; Navzenya, V. Y.; Kopylov, S. N.; Shebeko, D. Y.; Zamishevski, E. D. *Combust. Flame* **2000**, *121* (3), 542–547.

(5) Burcat, A.; Ruscic, B. *Third Millennium Ideal Gas and Condensed Phase Thermochemical Database for Combustion with Updates from Active Thermochemical Tables, ANL-05/20 and TAE 960*; Technion-IIT; Aerospace Engineering, and Argonne National Laboratory, Chemical Division, September 2005; p 11; ftp://ftp.technion.ac.il/pub/supported/aetdd/thermodynamics mirrored at http://garfield.chem.elte.hu/Burcat/burcat.html (accessed in June 2011).

(6) Csontos, J.; Rolik, Z.; Das, S.; Kallay, M. *J. Phys. Chem. A* **2010**, *114* (50), 13093–13103.

(7) Chase, M. W. *NIST-JANAF Thermochemical Tables*; 4th ed.; American Institute of Physics: New York, 1998.

(8) Ruscic, B.; Michael, J. V.; Redfern, P. C.; Curtiss, L. A. *J. Phys. Chem. A* **1998**, *102* (52), 10889–10899.

(9) Lias, S. G.; Bartmess, J. E.; Liebman, J. F.; Holmes, J. L.; Levin, R. D.; Mallard, W. G. Gas Phase Ion and Neutral Thermochemistry. *Journal of Physical Chemistry Reference Data*; NSRDS: U.S. Government Printing Office: Washington, DC, 1988; Vol. 17, Supplement 1.

(10) Natl. Bur. Stand. U.S. Tech. Note 270-3; 68.

(11) *Thermodynamic Properties of Pure Substances*; Glushko, V. P., Ed.; Izd. Nauka: Moscow, 1979.
(12) Papina, T. S.; Kolesov, V. P.; Golovanova, Y. G. *Russ. J. Phys. Chem.* **1982**, *56* (11), 2711–2714.
(13) Bickerton, J.; Minas da Piedade, M. E.; Pilcher, G. *J. Chem. Thermodyn.* **1984**, *16*, 661–668.
(14) Oren, M.; Iron, M. A.; Burcat, A.; Martin, J. M. L. *J. Phys. Chem. A* **2004**, *108* (38), 7752–7761.
(15) Marshall, P.; Srinivas, G. N.; Schwartz, M. *J. Phys. Chem. A* **2005**, *109* (28), 6371–6379.
(16) Wang, L. *J. Phys. Chem. A* **2008**, *112* (22), 4951–4957.
(17) Simm, I. G.; Danby, C. J.; Eland, J. H. D.; Mansell, P. I. *J. Chem. Soc. Faraday Trans. 2* **1976**, *72* (1), 426–434.
(18) Creasey, J. C.; Jones, H. M.; Smith, D. M.; Tuckett, R. P.; Hatherly, P. A.; Codling, K.; Powis, I. *Chem. Phys.* **1993**, *174* (3), 441–452.
(19) Hagenow, G.; Denzer, W.; Brutschy, B.; Baumgärtel, H. *J. Phys. Chem.* **1988**, *92* (23), 6487–6488.
(20) Baer, T.; Sztáray, B.; Kercher, J. P.; Lago, A. F.; Bodi, A.; Skull, C.; Palathinkal, D. *Phys. Chem. Chem. Phys.* **2005**, *7*, 1507–1513.
(21) Bodi, A.; Shuman, N. S.; Baer, T. *Phys. Chem. Chem. Phys.* **2009**, *11* (46), 11013–11021.
(22) Shuman, N. S.; Zhao, L. Y.; Boles, M.; Baer, T.; Sztáray, B. *J. Phys. Chem. A* **2008**, *112* (42), 10533–10538.
(23) Bodi, A.; Stevens, W. R.; Baer, T. *J. Phys. Chem. A* **2011**, *115* (5), 726–734.
(24) Walters, E. A.; Clay, J. T.; Grover, J. R. *J. Phys. Chem. A* **2005**, *109* (8), 1541–1547.
(25) Lago, A. F.; Kercher, J. P.; Bodi, A.; Sztáray, B.; Miller, B. E.; Wurzelmann, D.; Baer, T. *J. Phys. Chem. A* **2005**, *109*, 1802–1809.
(26) Clay, J. T.; Walters, E. A.; Grover, J. R.; Willcox, M. V. *J. Chem. Phys.* **1994**, *101* (3), 2069–2080.
(27) Asher, R. L.; Ruscic, B. *J. Chem. Phys.* **1997**, *106*, 210–221.
(28) Garcia, G. A.; Guyon, P. M.; Powis, I. *J. Phys. Chem. A* **2001**, *105* (36), 8296–8301.
(29) He, Y.-L.; Wang, L. *Struct. Chem.* **2009**, *20* (3), 461–479.
(30) Seccombe, D. P.; Tuckett, R. P.; Fisher, B. O. *J. Chem. Phys.* **2001**, *114* (9), 4074–4088.
(31) Werner, A. S.; Tsai, B. P.; Baer, T. *J. Chem. Phys.* **1974**, *60*, 3650–3657.
(32) Bodi, A.; Kercher, J. P.; Bond, C.; Meteesatien, P.; Sztáray, B.; Baer, T. *J. Phys. Chem. A* **2007**, *110* (50), 13425–13433.
(33) Borkar, S.; Ooka, L.; Bodi, A.; Gerber, T.; Sztáray, B. *J. Phys. Chem. A* **2010**, *114* (34), 9115–9123.
(34) Johnson, M.; Bodi, A.; Schulz, L.; Gerber, T. *Nucl. Instrum. Methods Phys. Res. A* **2009**, *610*, 597–603.
(35) Bodi, A.; Johnson, M.; Gerber, T.; Gengeliczki, Z.; Sztáray, B.; Baer, T. *Rev. Sci. Instrum.* **2009**, *80* (3), 034101.
(36) Eppink, A. T. J. B.; Parker, D. H. *Rev. Sci. Instrum.* **1997**, *68* (9), 3477.
(37) Baer, T.; Li, Y. *Int. J. Mass Spectrom.* **2002**, *219*, 381–389.
(38) Wiley, W. C.; McLaren, I. H. *Rev. Sci. Instrum.* **1955**, *26*, 1150–1157.
(39) Bodi, A.; Sztáray, B.; Baer, T.; Johnson, M.; Gerber, T. *Rev. Sci. Instrum.* **2007**, *78* (8), 084102.
(40) Sztáray, B.; Baer, T. *Rev. Sci. Instrum.* **2003**, *74*, 3763–3768.
(41) Sztáray, B.; Bodi, A.; Baer, T. *J. Mass Spectrom.* **2010**, *45* (11), 1233–1245.
(42) *Gaussian 09*, Revision A.1; Gaussian, Inc.: Wallingford, CT, 2009.
(43) Raghavachari, K.; Stefanov, B. B.; Curtiss, L. A. *J. Chem. Phys.* **1997**, *106* (16), 6764–6767.
(44) Curtiss, L. A.; Redfern, P. C.; Raghavachari, K. *J. Chem. Phys.* **2007**, *126*, 084108.
(45) Tajti, A.; Szalay, P. G.; Csaszar, A. G.; Kallay, M.; Gauss, J.; Valeev, E. F.; Flowers, B. A.; Vazquez, J.; Stanton, J. F. *J. Chem. Phys.* **2004**, *121* (23), 11599–11613.
(46) Becke, A. D. *J. Chem. Phys.* **1993**, *98*, 5648–5652.
(47) Zhao, Y.; Truhlar, D. G. *Theor. Chim. Acta* **2008**, *120* (1−3), 215–241.
(48) Wilson, A. K.; Woon, D. E.; Peterson, K. A.; Dunning, T. H. *J. Chem. Phys.* **1999**, *110* (16), 7667–7676.
(49) Martin, J. M. L.; Sundermann, A. *J. Chem. Phys.* **2001**, *114* (8), 3408–3420.
(50) Peterson, K. A.; Figgen, D.; Goll, E.; Stoll, H.; Dolg, M. *J. Chem. Phys.* **2003**, *119* (21), 11113–11123.
(51) Martin, J. M. L.; de Oliveira, G. *J. Chem. Phys.* **1999**, *111*, 1843–1856.
(52) Montgomery, J. A.; Frisch, M. J.; Ochterski, J. W.; Petersson, G. A. *J. Chem. Phys.* **2000**, *112* (15), 6532–6542.
(53) Wahrhaftig, A. L. *J. Chem. Phys.* **1942**, *10* (4), 248.
(54) Schmitz, H.; Schumacher, H. J. *Z. Naturforsch. A* **1947**, *2* (6), 359–362.
(55) Dibeler, V. H.; Walker, J. A.; McCulloh, K. E. *J. Chem. Phys.* **1970**, *53* (12), 4414–4417.
(56) Nordine, P. C. *J. Chem. Phys.* **1974**, *61* (1), 224–226.
(57) Coxon, J. A. *Chem. Phys. Lett.* **1975**, *33* (1), 136–140.
(58) McDermid, I. S. *J. Chem. Soc., Faraday Trans. 2* **1981**, *77*, 519–530.
(59) Ochterski, J. W.; Petersson, G. A.; Montgomery, J. A. *J. Chem. Phys.* **1996**, *104* (7), 2598–2619.
(60) Forysinski, P. W.; Zielke, P.; Luckhaus, D.; Signorell, R. *Phys. Chem. Chem. Phys.* **2011**, *12*, 3121–3130.
(61) Chau, F. T.; McDowell, C. A. *J. Electron Spectrosc. Relat. Phenom.* **1975**, *6* (5), 357–363.
(62) Wang, F. C. Y.; Leroi, G. E. *Ann. Isr. Phys. Soc.* **1983**, *6*, 210.
(63) Skorobogatov, G. A.; Dymov, B. P.; Nedozrelova, I. V. *Zh. Obshch. Khim.* **1996**, *66* (11), 1824–1833.
(64) Dymov, B. P.; Skorobogatov, G. A.; Khripun, V. K. *Zh. Fiz. Khim.* **1991**, *65* (8), 2085–2093.
(65) *NIST Chemistry WebBook, NIST Standard Reference Database Number 69*; February 2000 ed.; National Institute of Standards and Technology: Gaithersburg, MD, 2005.
(66) Troe, J.; Ushakov, V. G.; Viggiano, A. A. *J. Phys. Chem. A* **2006**, *110* (4), 1491–1499.
(67) Stevens, W.; Sztáray, B.; Shuman, N. S.; Baer, T.; Troe, J. *J. Phys. Chem. A* **2008**, DOI: 10.1021/jp807930k.
(68) Shuman, N. S.; Miller, T. M.; Viggiano, A. A.; Troe, J. *J. Chem. Phys.* **2011**, *134* (9), 094310.
(69) Song, Y.; Qian, X.-M.; Lau, K.-C.; Ng, C. Y. *J. Chem. Phys.* **2001**, *115*, 4095–5003.
(70) Ruscic, B. *Active Thermochemical Tables*, early beta 1.110, retrieved on July 14, 2011.